Journal of Nuclear Materials 588 (2024) 154830

Contents lists available at ScienceDirect

Journal of Nuclear Materials

journal homepage: www.elsevier.com/locate/jnucmat

Numerical and experimental development of cupronickel filler brazed joints for divertor and first wall components in DEMO fusion reactor

V. Díaz-Mena [a,*], J. de Prado [a], M. Roldán [b], I. Izaguirre [a], M. Sánchez [a], M. Rieth [c], A. Ureña [a]

[a] Materials Science and Engineering Area, ESCET, Rey Juan Carlos University, C/Tulipán s/n Móstoles, 28933, Madrid, Spain
[b] Division of Fusion Technologies, National Fusion Laboratory, CIEMAT, Avenida Complutense, 40, 28040, Madrid, Spain
[c] Karlsruhe Institute of Technology, Institute for Applied Materials, Hermann-von-Helmholtz-Platz 1 Eggenstein-Leopoldshafen 76344, Karlsruhe, Germany

GRAPHICAL ABSTRACT

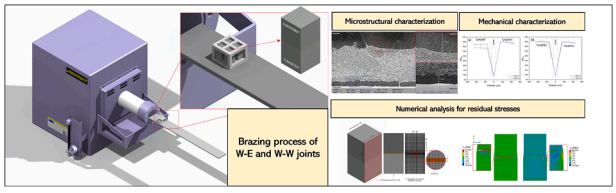

ARTICLE INFO

Keywords:
Brazing
Fusion reactor
Tungsten
EUROFER 97
ANSYS

ABSTRACT

The brazeability of a cupronickel commercial alloy (Cu10Ni) was evaluated for its use as a filler alloy for high-temperature joining of tungsten to the reduced activation ferritic/martensitic steel EUROFER 97 (W-E) and between tungsten base materials (W-W) for its application at the first wall and divertor of future fusion reactors. In addition, given the importance of the residual stresses in these heterogenous joints, a study of the brazing conditions and the impact of the selected filler has been conducted using numerical software to understand its impact on the quality of the joint.

Two thermal cycles were evaluated (1165 °C and 1190 °C) and selected based on the thermal characterization of the filler alloy. The microstructural examination revealed that, in W-E joints, nickel acts as an activator element, reacting and forming interfacial layers at the EUROFER 97 - Cu10Ni interface. In the case of the W-W joints, a lower level of diffusion phenomenon and metallurgical interaction between Cu10Ni and base materials were observed. The hardness profile indicated that the hardening process of EUROFER 97 was associated with the formation of untempered martensite. On the other hand, tungsten kept the received hardness. The mechanical characterization by shear test reported similar values between both types of joints carried out at 1190 °C but different when the temperature was increased (1165 °C), associated with the brittle character of tungsten and its lower metallurgical interaction.

The numerical analysis of the brazing process carried out with ANSYS software shows that residual stresses are accumulated mainly at the interfaces. The information provided by the simulation shows, for a 50 μm filler thickness, the importance of mitigating the residual stress by selecting a filler with an intermediate Coefficient of Thermal Expansion (CTE) that alleviates mechanical stresses relative to the base materials.

* Corresponding author.
E-mail address: victor.diaz@urjc.es (V. Díaz-Mena).

https://doi.org/10.1016/j.jnucmat.2023.154830
Received 22 September 2023; Received in revised form 20 November 2023; Accepted 20 November 2023
Available online 22 November 2023

1. Introduction

Due to the increase in population and the constant technological development experienced by humans, the demand for electricity worldwide has increased in recent decades and is expected to increase considerably. However, the still high dependence on fossil fuels and the pollution they cause is forcing researchers to develop new renewable energy sources to replace traditional ones. Nuclear fusion energy is the most promising energy source for the future to obtain clean energy without carbon emissions and featuring a closed fuel cycle [1].

From a materials science and engineering perspective, one of the key points is the selection and manufacturing of both the fusion reactor's structural materials and the Plasma Facing Materials (PFMs) [2,3]. Developing new advanced materials or new processing techniques represents one of the strategic keys to the successful development the proposed fusion energy reactors, which will operate under unprecedented fluxes of high-energy neutrons and intense static and dynamic thermomechanical stresses. These materials can improve the reactor performance by increasing strength, creep resistance, and superior corrosion and neutron radiation damage resistance, thus expanding the operational reactor window [4–6].

For the first wall structural applications, R&D of Reduced Activation Ferritic Martensitic Steels (RAFMS) has been widely studied and EUROFER 97 [7] or the F82H [8] have been the main options considered for design and experiments. Due to the presence of Cr-rich particles in these RAFMS, which result in lower creep resistance [9], other types of steels like Oxide Dispersed Steels (ODS) are being studied for future applications [10].

For the PFMs, the most promising and studied materials currently are tungsten and its alloys for the first wall [11–13]. Specifically, one of the components exposed to the most severe conditions among all PFMs (such as high thermal loads, neutron irradiation and particles exposure [14]) is the divertor. In a mono-block divertor, tungsten not only plays the role of armor material but also the role of structural material due to its many suitable properties, such as high melting point, low sputtering rate, reasonable thermal conductivity and high strength [15,16].

This reactor's multi-component configuration is the reason why the development of joining technologies between dissimilar materials is an unresolved issue that needs further study. High-temperature brazing is widely used as a possible solution that mitigates the problem of joining tungsten to steel (W-E) and to itself (W-W) for the first wall and divertor applications. The advantages of this technique include: using lower joining temperatures than those of liquid-state joining techniques, and shorter times than those of solid-state joining.

The filler material must be carefully chosen to fulfill general requirements such as high spreading capabilities, chemical compatibility, and specific requirements. Both copper and nickel elements are commonly used in brazing alloys because of their high strength, high thermal conductivity, and corrosion resistance at the high temperatures of the joints. When used for a fusion reactor, both materials can help improve the joint's structural integrity and ability to withstand the high temperatures and pressures in a fusion reactor by accommodating residual stresses [17]. These residual stresses are primarily due to the mismatch between coefficients of thermal expansion (CTEs) of the individual materials, the mismatch of the material's elastic properties and the plastic flow of the filler metal [18]. The residual stresses affect the strength of the joint during environmental mechanical or thermal loading and, in some cases, lead to catastrophic failure during the brazing process by crack propagation along or near an interface, explaining why careful selection of the filler metal and investigation of stress levels along potential failure interfaces is crucial. To this end, as the final step in the characterization of this paper, Finite Element Analysis (FEA) is used to investigate the residual stresses during the cooling from the brazing temperature to room temperature of a W-E joint and a W-W joint.

Researchers from the Nuclear Fusion Community have developed brazing processes between materials such as EUROFER 97 and tungsten and its alloys (W-Cr-Y) with Cu and Cu-based alloys as filler for years [19–22]. Additionally, the use of pure copper and different copper-based alloys (Cu-20Ti, Cu-Ge) as fillers has been extensively studied for these joints.

For W-E joints, Zhong et al. [23] studied the effect of brazing temperature on the microstructure of these joints using pure nickel as a filler. A diffuse interlayer was observed, where elements such as chromium or iron did not form different phases with nickel. This effect could be attributed to the proper compatibility between steel and nickel, which can be predicted by the Fe-Ni and Cr-Ni phase diagrams, where the solubility of nickel in iron at welding temperatures is very similar to that of chromium. Therefore, a solid solution with a gradual element distribution is formed at the interface.

The interaction between nickel and tungsten is also particularly interesting, especially in W-W joints, where nickel cannot diffuse into tungsten. In these joints, Sánchez et al. [24] observed that at the interface with tungsten in W-W joints, some spherical tungsten particles were incorporated into the braze. The authors indicate that a dilution phenomenon could have occurred between the molten filler material and the tungsten, which progressed preferentially along the grain boundaries of the base material, followed by a partial dissolution of the tungsten grains. This is generally associated with constitutional liquefaction and grain migration phenomena.

Similar to copper, Ni-Ti alloys have also been studied for application in fusion power plants. For example, Cai et al. [17] proposed a new way to join W to steel using the Ti/Ni/Ti combination as an interlayer through diffusion brazing. During the process, a complex reaction layer consisting of TiC, TiFe, $TiFe_2$, $TiCr_2$, and TiNi was identified at the Ni/steel interface.

This paper explores the brazeability and complete characterization of W-E and W-W joints using a Cu-Ni commercial filler alloy (Cu10Ni). Initially, a complete characterization of the filler in the as-received state was conducted, followed by an examination of different brazing parameters such as joining temperature and its discussion based on existing literature. This filler composition demostrated promising results in both operational and metallurgical brazeability terms.

Moreover, the study of joint formation is complemented by Finite Element Analysis (FEA) of the cooling process from brazing temperature inside the furnace for a W-E joint to understand the residual stresses produced in the materials. This last study is a novel aspect of the characterization and is significant as the thermal stresses produced during the joint processing are one of the main concerns for the successful design of the joint and future operation in the reactor. Additionally, manufactured joints with lower residual stresses are expected to generate lower thermal stresses during operation, thereby extending the component's operational life. Therefore, FEA conducted as the final step in characterizing the brazed joints using ANSYS Workbench software. For this evaluation, a 2D CAD model representing joint between base materials of 3×2 mm^2 with a 50 μm-thickness filler was designed using ANSYS SpaceClaim software.

2. Experimental procedure

2.1. Base materials

The base materials used for the bonding were: i) tungsten (>99.97%, Plansee); and ii) a reduced activation ferritic/martensitic steel (EUROFER 97) with a chemical composition in wt.% of 0.11C, 8.90Cr, 0.42Mn, 0.19 V, 1.10 W, 0.14Ta, and Fe balance [25].

2.2. Filler materials

The intermediate material used as filler was a commercial cupronickel alloy supplied by Auerhammer Metallwerk named Cu10Ni with a chemical composition specified by the manufacturer in wt.% of ≤ 11Ni,

$\leq$ 0.1Fe, $\leq$ 0.3Mn and Cu balance. The filler material was received as a sheet 4 × 3 cm^2 and 600 μm thick.

2.3. Brazing process

Before the joining tests, base materials were prepared as follows. First, cutting them to the dimension of 5 × 5 × 5 mm^3, then grinding the exposed surfaces from grit size P800 to P4000 with silicon carbide papers to control the surface roughness, and, finally, cleaning the polished surfaces with isopropanol.

A tubular furnace (*Nabertherm RHTC 80–450/15*) connected to a turbomolecular vacuum chamber (*Pfeiffer VACUUM TSM 071 E*) was used for brazing at a residual pressure of 10^{-6} mbar. The disposition of the materials employed inside the furnace is shown in Fig. 1. Brazing was performed by applying the following cycle: i) a heating ramp from room temperature to the chosen brazing temperature at 5 °C/min rate, ii) dwell time of 10 min at the selected temperature, and iii) cooling ramp to room temperature also at 5 °C/min rate. As a result, brazing temperatures were 25 and 50 °C over the experimental liquidus temperature of the filler (1165 and 1190 °C), which according to previous studies carried out by researchers of the area, is high enough to achieve a complete filling of the joint clearance and to establish a chemical and physical phenomenon to enhance adhesion properties at the interface [19,22,24].

2.4. Characterization techniques

The Liquidus temperature of the filler was determined by Differential Thermal Analysis (*DTA, Setaram Thermic Analyzer Setsys 16/18*) in an argon atmosphere. The experiment consisted of a 5 °C /min heat ramp from room up to 100 °C above the theoretical liquidus temperature. Then, the samples were cooled down using the same ramp. The heat exchanges during the heating and cooling processes were recorded.

The composition of the filler material was also determined by X-ray fluorescence Spectroscopy (XRF, *Philips Magix Pro*) for comparison with the composition provided by the manufacturer in the specification sheet.

These two characterization techniques were used with the main intention of confirming two key parameters of brazing process: liquidus temperature and melting range. Therefore, DTA analyses were carried out to determine differences between the information obtained experimentally by the laboratory and the one provided by the manufacturer. In that case, is it important to know the differences in composition that would justify this deviation by a fluorescence or spectroscopy analysis.

The samples were metallographically prepared following the standard polishing technique: i) grinding from grit size P800 to P4000 with silicon carbide and ii) polished with 1 and 3 μm diamond suspension. Then, the cross-section microstructural analysis of the brazed samples was performed using Scanning Electron Microscopy at 20 keV (SEM, *S3400 Hitachi*) equipped with an Energy Dispersive X-Ray (EDX, *Quantax*) analyzer. In addition, to distinguish some microstructural features more clearly, a Field Emission Gun Scanning Electron Microscope at 30 keV (FEG-SEM, *Auriga Zeiss*) with an in-lens detector for secondary and backscatter electrons was used.

The mechanical properties of the joints were evaluated through microhardness and shear tests. The hardness study was carried out by tracing a profile across the joints with *MHV-2SHIMADZU* equipment. This study explains the brazing process's effect on the base materials' hardness properties. A 100 g ($HV_{0.1}$) load was applied for 30 s following the *ASTM: E384–11 Standard Test Method for Knoop and Vickers Hardness of Materials*. Three measurements were performed for each position with distances between neighbor indentations longer than three times the residual imprint sizes.

Shear strength values were obtained using a shear fixture between compress plates in a Universal Testing Machine (*Zwick Z100*) at a 1 mm/min speed. Several samples for each condition were measured to determine the strength properties of the joints.

2.5. FEA pre-processing

2.5.1. Material properties

All materials were defined with the following temperature-dependent properties:

- Mechanical properties: the elastoplastic properties as a function of temperature were defined with different actual stress-strain curves covering the whole range of the thermal process operational window [11,12,25–28]. Missing data were completed using an adjustment with the "cftool" option of the Matlab R2021.
- Thermo-physical properties: density and coefficient of thermal expansion, specific heat, and thermal conductivity were obtained from several sources [11,12,25–28] and determined using JMatPro software.

2.5.2. CAD model and discretization

The 2D CAD model was created in ANSYS SpaceClaim, and the meshing for FE analysis was in ANSYS Workbench 2021 R2. The node elements are based on PLANE183, a configuration suitable for plasticity, hyperelasticity, creep, stress stiffening, large deflection, and large strain phenomena, varying on vertical and horizontal edges. The number of elements (NE) along with the Bias Factor (BF) of base materials and filler edges are shown in Fig. 2. The 2D model was preferred over the 3D model for saving analysis time and, considering the symmetry of the

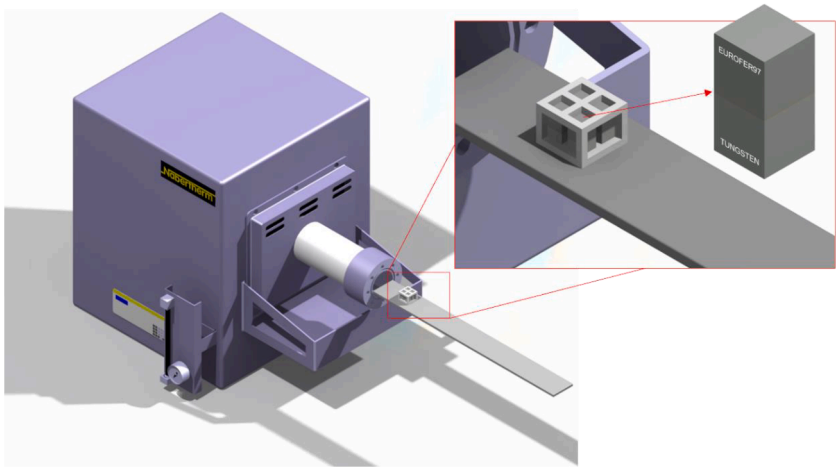

Fig. 1. Arrangement of the materials inside the tubular furnace in 5 × 5 × 5 cm^3 cubes inside a tool prepared for better support.

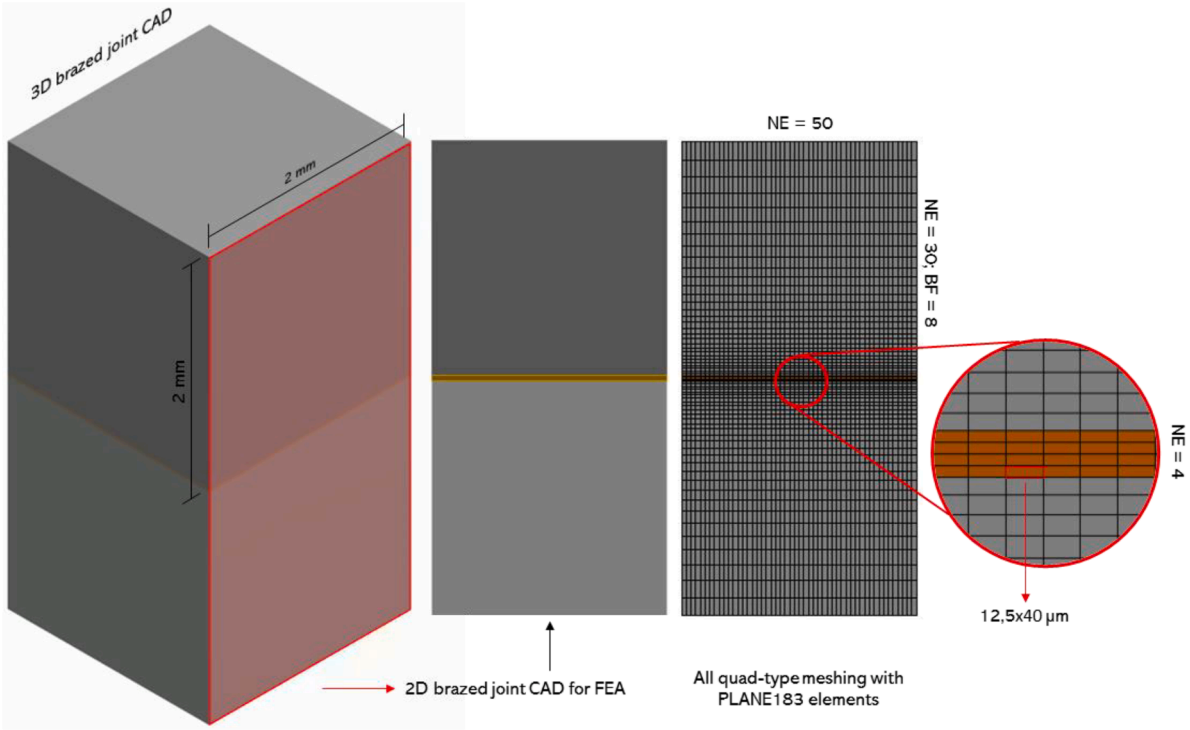

Fig. 2. CAD model and meshing used for FE analysis. The number of elements (NE) and bias factor (BF) of the vertical and horizontal edges are marked.

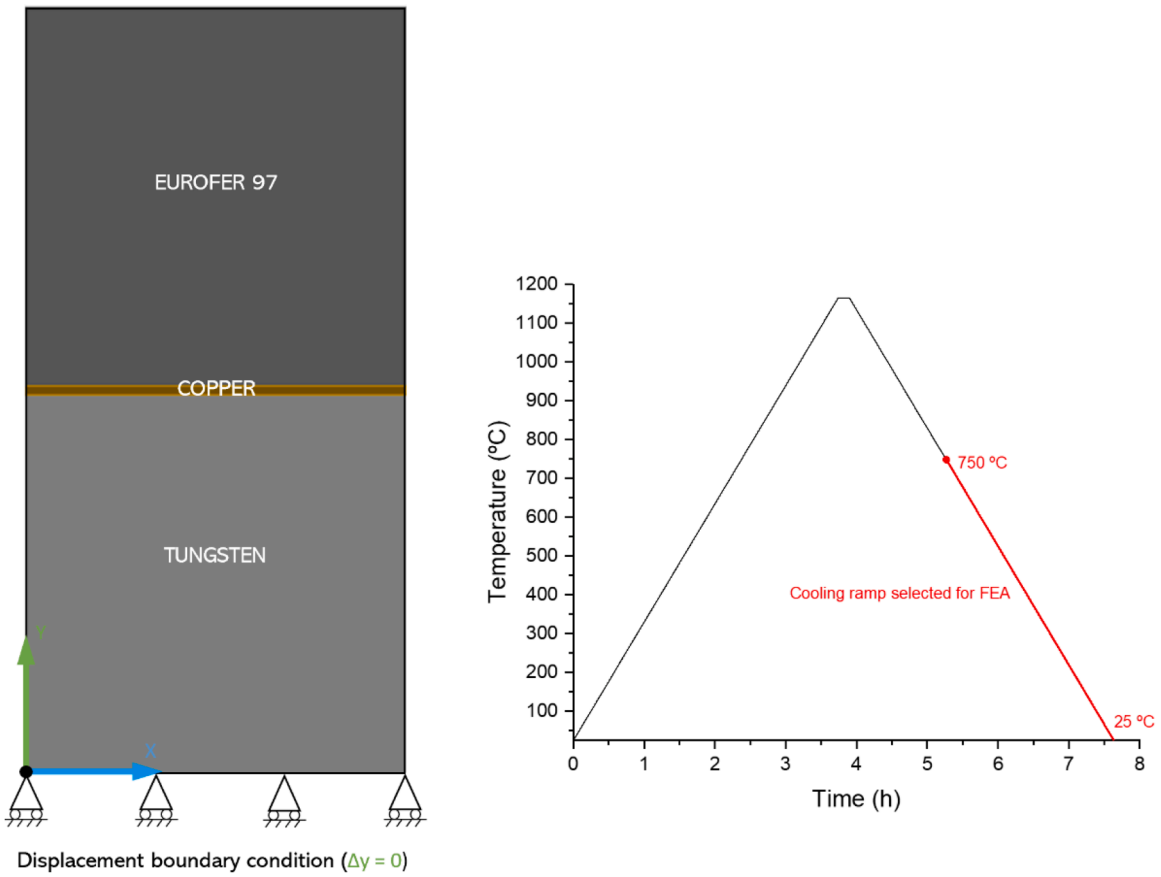

Fig. 3. Boundary conditions imposed on the brazed joint between materials and the cooling ramp selected for FEA.

model, the results of a 2D section apply to the whole.

2.5.3. Boundary conditions

The boundary condition applied on the body was the support seen in Fig. 3 on the underside of the tungsten base material ($\Delta Y = 0$). A Transient Structural analysis model was used for the stress analysis during the cooling ramp inside the furnace. Despite radiation phenomena being the physical mechanism for the heat transfer between the materials and the inside of the furnace, an internal temperature ramp with no thermal gradient ($\Delta T = 0$ in each material) was applied to the three bodies in this analysis (Fig. 3). This decision is based on the low dimensions of the model and the emissivity values for the three materials, where hardly any thermal gradient appears. The temperature ramp was a cooling ramp from 750 °C to 25 °C because no stress-strain curves were found at temperatures above 750 °C.

3. Results

3.1. Microstructural and mechanical characterization of the cupronickel alloy

Before the brazing study, the commercial filler was compositionally, microstructurally, and thermally characterized in as-received conditions to determine the experimental values and properties necessary to develop the brazing study.

Table 1 shows the experimental composition in wt.% of the filler obtained by XRF analysis and its correlation with that provided by the manufacturer. The results indicated some minor deviations in the copper and nickel content. However, no iron was measured in the filler.

The microstructure of the filler, shown in Fig. 4a, consists of equiaxial grains without preferential orientation and free of apparent twins, characteristic of these alloys. The presence of some inclusions is probably associated with the low iron and manganese content. The microstructure was examined by etching with 50 ml of distilled water and 50 ml of HNO_3 during 10 s.

The thermal behavior of the commercial Cu-Ni filler used during the brazing process was characterized by DTA. These thermograms were recorded during heating and cooling from room temperature to 1300 °C (Fig. 4b). During the cooling phase, between 1000 °C and 1200 °C, two exothermic peaks related to the alloy's melting process can be observed. As the temperature decreases, the peaks take place in the range of 1140 °C – 1131 °C and 1055 °C – 1045 °C, with 1140 °C the liquidus temperature of the alloy at which the filler is entirely melted. This confirms the information provided by the manufacturer and, due the negligible deviation in terms of liquidus temperature was found, no further composition analysis beyond XRF was necessary.

Finally, the hardness of Cu10Ni commercial filler was measured, obtaining a value of 148 ± 10 $HV_{0.1}$. The initial thickness of the filler was 600 μm, which would result in an undesirably wide seam after brazing. Therefore, it was laminated up to 200 μm, facilitating the stacking of materials when placed in the oven for welding. This cold-rolled process causes plastic deformation reducing the initial grain size (as it raises the density of defects such as dislocations within the matrix) and increasing its strength and hardness. The microstructure of the filler laminated is shown in Fig. 5, where the preferential rolling direction (RD) could be observed. The hardness value after rolling was 158 ± 10 $HV_{0.1}$.

Table 1
Comparison study between the composition of Cu10Ni filler specified by the manufacturer and measured by XRF.

	Cu (wt.%.)	Ni (wt.%.)	Fe (wt. %.)	Mn (wt.%.)
Specification sheet	88.60	11.00	0.10	0.30
XRF	89.30 ± 0.09	10.40 ± 0.03	–	0.257 ± 0.04

3.2. Microstructural characterization of W-E joints after two different brazing cycles

The first attempt to join W to EUROFER 97 using Cu-Ni filler was carried out using the laminated filler at 1165 °C. The resultant joint shows high metallic continuity along both E-Cu10Ni and W-Cu10Ni interfaces (Fig. 6a). Furthermore, the filler has correctly melted at the brazing temperature and filled the whole joint clearance, establishing metallurgical interactions with EUROFER 97 and tungsten through diffusion processes and partial dilution of the base materials in a solid state. This process allows operational brazeability, forming an approximately 92 μm thick braze zone.

The second brazing attempt used 50 °C over the experimental liquidus temperature (1190 °C - Fig. 6c). Again, both metallic and operative brazeability was also achieved. However, the thickness of the brazing seam is reduced, in this case, up to 63 μm. The reduction is associated with the lower viscosity of the filler at this temperature which promotes the liquid filler's exudation out of the joint clearance, a phenomenon facilitated by capillarity forces.

The element distribution of the brazed joints can be seen in Fig. 6b and d for the lower and higher brazing temperatures, respectively. Both joints show a homogeneous distribution of nickel and copper elements through the braze thickness, especially in the lower brazing temperature sample. Both samples, but mainly in the joint brazed at 1190 °C, show the formation of a nickel enrichment layer in the E-Cu10Ni interface and some nickel-rich phases inside the braze area. This enrichment will be further analyzed and discussed in Section 4.1.

The W-Cu10Ni interface showed an entirely different metallurgical behavior and low metallurgical interaction between elements. However, isolated nickel-rich phases were found in the 1190 °C condition.

A more exhaustive study of the microstructure developed for the 1190 °C condition was performed using a Field Emission Gun Scanning Electronic Microscope (FEG-SEM). The high-resolution image of the brazed joint, etched with 50 ml of distilled water and 50 ml of HNO_3, is shown in Fig. 7 and a more detailed EDX mapping divided by elements of this brazing condition is shown in Fig. 8. These images allow the identification of a complex heterogeneous microstructure formed by different phases. EDX composition analysis showed that the braze is constituted by a copper-rich matrix and dark tonality copper-rich precipitates inside the matrix with round geometry.

Line scan and punctual analysis were performed at the E-Cu10Ni interface to complete the characterization. The line scan analysis is shown in Fig. 9b, where Cu, Ni, Fe, and W composition is measured as it penetrates the diffusion zone from the EUROFER 97 base material, as indicated in Fig. 9a. A semiquantitative composition determination of different points corresponding with the line scan studied area was carried out by EDX punctual analysis as shown in Fig. 10. It indicates a similar atomic% of Cu and Ni, slightly higher for the latter, at the center of the diffusion layer (point number 2 in Fig. 10).

3.3. Microstructural characterization of W-W joints

W-W joints using Cu10Ni filler after the thermal brazing process with a thickness of 198 μm are shown in Fig. 11a and 15 μm in Fig. 11b at 1165 °C and 1190 °C, respectively.

The brazed joints' general composition and element distribution can be seen in Fig. 12a and Fig. 12b for the temperature conditions of 1165 °C and 1190 °C, respectively. The compositional mapping does not show the formation of diffusion zones at the interfaces nor the formation of secondary phases or aggregates in the braze, so it seems to be constituted by a unique solid solution phase.

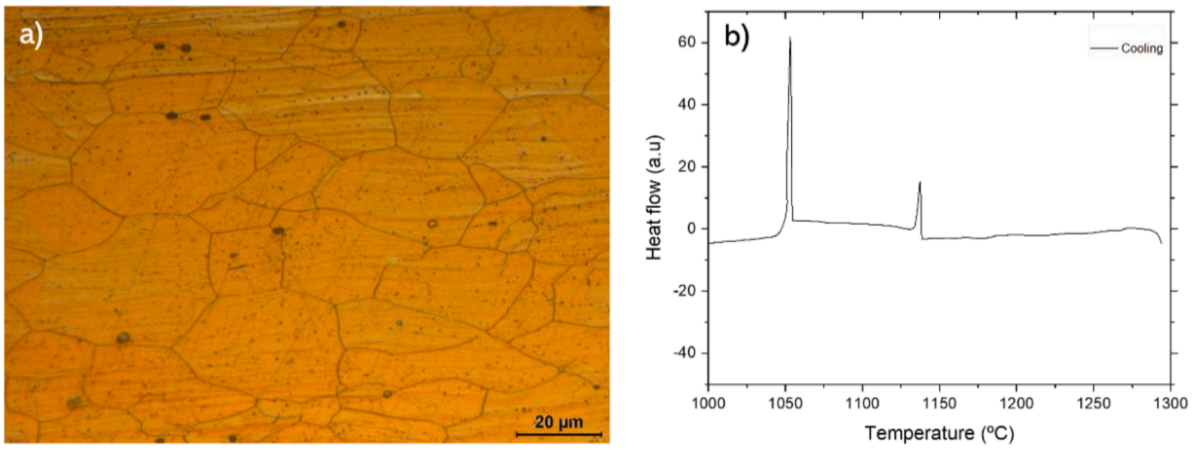

Fig. 4. a) Optical micrograph of Cu10Ni commercial filler microstructure revealed by etching with 50 ml of distilled water and 50 ml of HNO_3 and b) cooling curve of differential thermal analysis for Cu10Ni commercial filler.

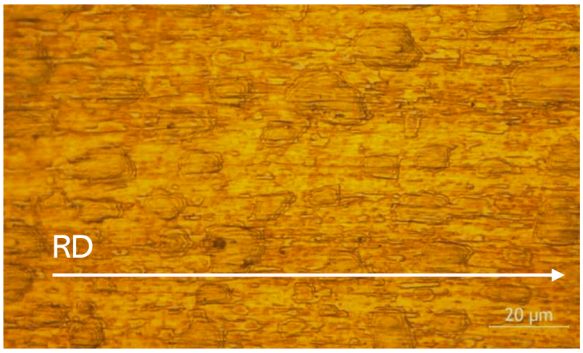

Fig. 5. Micrograph of Cu10Ni commercial filler laminated to 200 µm revealed by etching with 50 ml of distilled water and 50 ml of HNO_3.

3.4. Mechanical properties of the joints

Microhardness and shear strength tests were carried out on the mechanical characterization of brazed joints. The first characterization aims to determine the effect of the different brazing conditions on the base material properties by tracing a hardness profile from one base material to the other. For example, different hardness values could be associated with the solubilization of precipitates, grain growth, phase transformation, etc. The latter aims to determine the maximum strength of withstanding the joint under a shear mode load.

Fig. 13a and b show the hardness values evolution of the brazed joint treated at 1165 and 1190 °C for both types of joints, W-E and W-W joints, respectively. Dashed lines represent the joint-base material interfaces. In all joints, the hardness value of tungsten remains approximately constant at an average value of 450 ± 4 $HV_{0.1}$, which is almost equal compared to the starting value of 456 ± 5 $HV_{0.1}$.

In the W-E joints, EUROFER 97 base material shows a hardness variation related to the brazing conditions used. The measured hardness increases to 423 ± 3 $HV_{0.1}$ for 1165 °C and 382 ± 2 $HV_{0.1}$ for 1190 °C. The as-received hardness of EUROFER 97 was 225 ± 3 $HV_{0.1}$ [25]. The filler values are about 100 ± 3 $HV_{0.1}$ for both types of cycles in both types of joints carried out, which is lower than the initial measured value of 158 ± 10 $HV_{0.1}$ of the laminated filler and even the as-receive filler hardness.

Shear test values are shown for all brazing conditions and joints in Fig. 14, where the error bars show the standard deviation obtained for each composition in the tests. Values for the 1190 °C conditions are very similar for both W-W and W-E brazed joints, with values around 168 ± 14 MPa for W-W and 164 ± 37 MPa for W-E. However, this is not the case for 1165 °C conditions, where the obtained strengths are 174 ± 32 MPa and 157 ± 21 MPa for the W-E and W-W brazed joint, respectively.

Fig. 15 shows the fracture surface of W-E at 1165 °C condition as representative of all tests due to the similarities found in the fracture mechanisms in all conditions. In all conditions, cracks were initiated and propagated through the W-Cu10Ni interface, which made the fracture surface appreciable in Fig. 15. The W-side fracture surface analysis showed an intergranular fracture mechanism in some regions where tungsten base material is appreciated. In the other regions, Cu-Ni solid solution appears as a cohesive fracture phenomenon of the brazed joint. There is no presence of EUROFER 97 in none of the two fracture surfaces, which confirms that cracks started at the W base material and then propagated through the W-Cu10Ni interface. In Section 4, a discussion about the more brittle W-Cu10Ni interface will be carried out to explain this phenomenon.

4. Discussion

4.1. Mechanism formation and microstructural evolution of W-E joints

The nickel-rich layer at the E-Cu10Ni interface as shown and commented on Fig. 6c could be associated with dilution and diffusion phenomena between the braze and the base material. The higher temperature sample shows a more pronounced layer because dilution and solid-state diffusion processes are promoted as the temperature increases.

The precipitates shown in Fig. 7 could have been formed because of a dilution process during the liquid state of the braze. Iron and chromium were dissolved from the EUROFER 97 base material and precipitated during the cooling stage due to the decrease in solubility of those elements in copper as illustrated by the equilibrium phase diagram shown in Fig. 16. However, in some areas of the braze (as seen in Fig. 7a and Fig. 7b the microstructure formed seems to have a eutectic morphology.

Both interfaces mentioned in Fig. 7, concerning the top and bottom interfaces of the joint, have been studied and discussed in detail. Their microstructures were formed in both liquid and solid states. In the case of the E-Cu10Ni interface, a diffusion region of approximately 15 ± 3 µm can be observed, marked with a white arrow in the red box of Fig. 7. In the case of the W-Cu10Ni interface, the presence of a layer rich in Ni-Fe-Cr of 7 µm is formed (as seen in Fig. 7b). The formation of this layer could be associated with the incorporation of Fe in the braze and the heterogeneous solidification, during cooling, of the Ni-Fe-Cr rich phase observed. This last layer and the diffusion layer have a similar composition and element distribution as indicated by the element distribution map in Fig. 8 shows.

Concerning the diffusion layer of the E-Cu10Ni interface, it has been

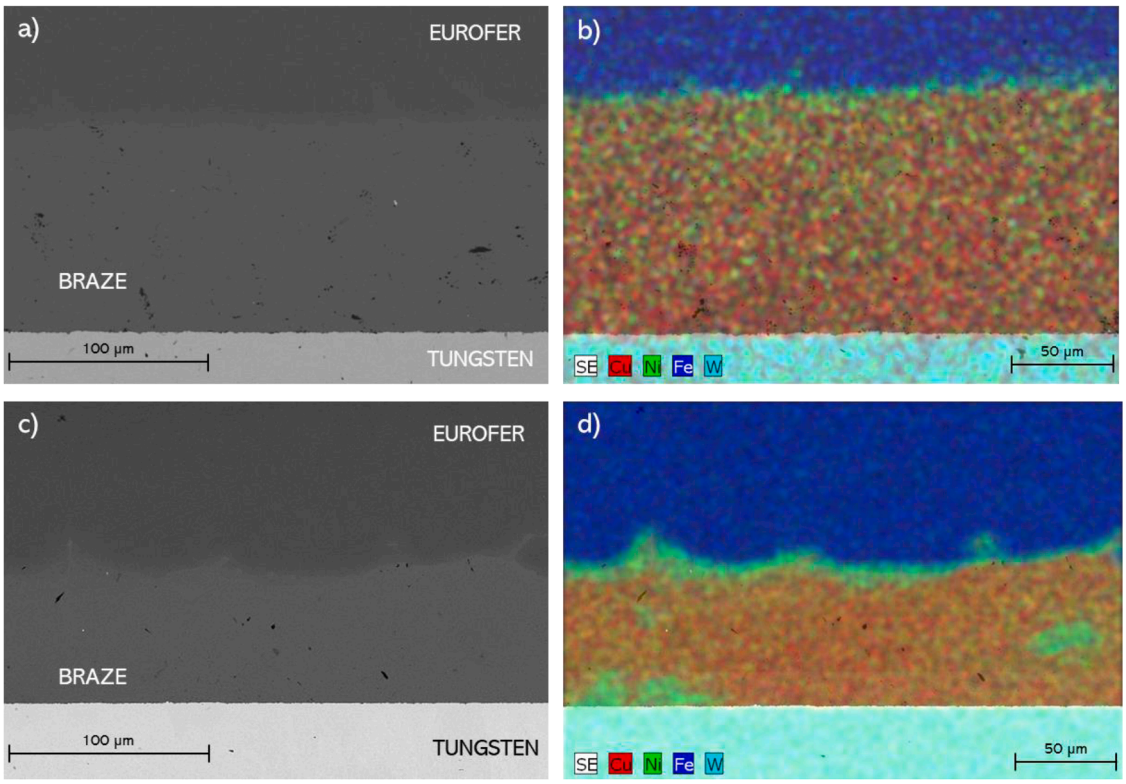

Fig. 6. W-E joints brazed with Cu10Ni commercial filler at 1165 °C (a,b) and 1190 °C (c,d).

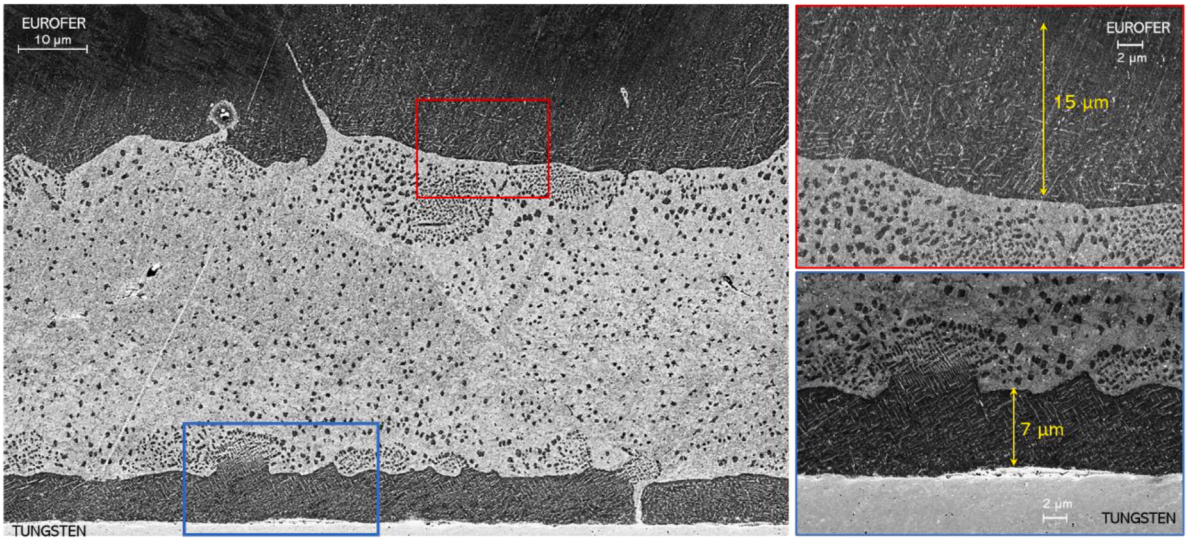

Fig. 7. FEG-SEM micrographs of the brazed joint at 1190 °C with details of the top surface (red square) and the bottom (blue square).

formed by the solid-state diffusion mechanism of copper and nickel in the iron crystalline structure. As the nickel solubility in iron is high [29], this element remains in a solid solution after cooling, but the reduced solubility of copper in iron results in copper precipitates forming rod-like precipitates. In addition to the diffusion phenomenon, the interface is characterized by the interaction of the liquid braze with the base material giving rise to a "wave" profile in which the liquid braze has punctually penetrated the base material following austenitic grain boundaries due to grain boundaries liquefaction process (marked with a white arrow in Fig. 7).

All analyses carried out in and Figs. 7 and 9 show that at the center of the brazed joint and the bottom W-Cu10Ni interface, iron and chromium are detected, even though the filler itself does not contain these elements. The presence of those elements, especially at the W-Cu10Ni interface, could be associated with the dilution phenomena of the EUROFER 97 in the braze at high temperature, which subsequently initiates the precipitation phenomenon giving rise to the formation of the eutectics aggregates as the temperature decreases, according to the previous discussion.

Considering the Fe-Cu-Ni ternary phase diagram [30] shown in Fig. 16, the composition of the point marked as 2 in Figs. 7 and 11, corresponds to the center of the diffusion layer, has its liquid phase between 1350 and 1400 °C, while compositions marked as 3 and 4, corresponding to the nearest zone of the braze with the E-Cu10Ni

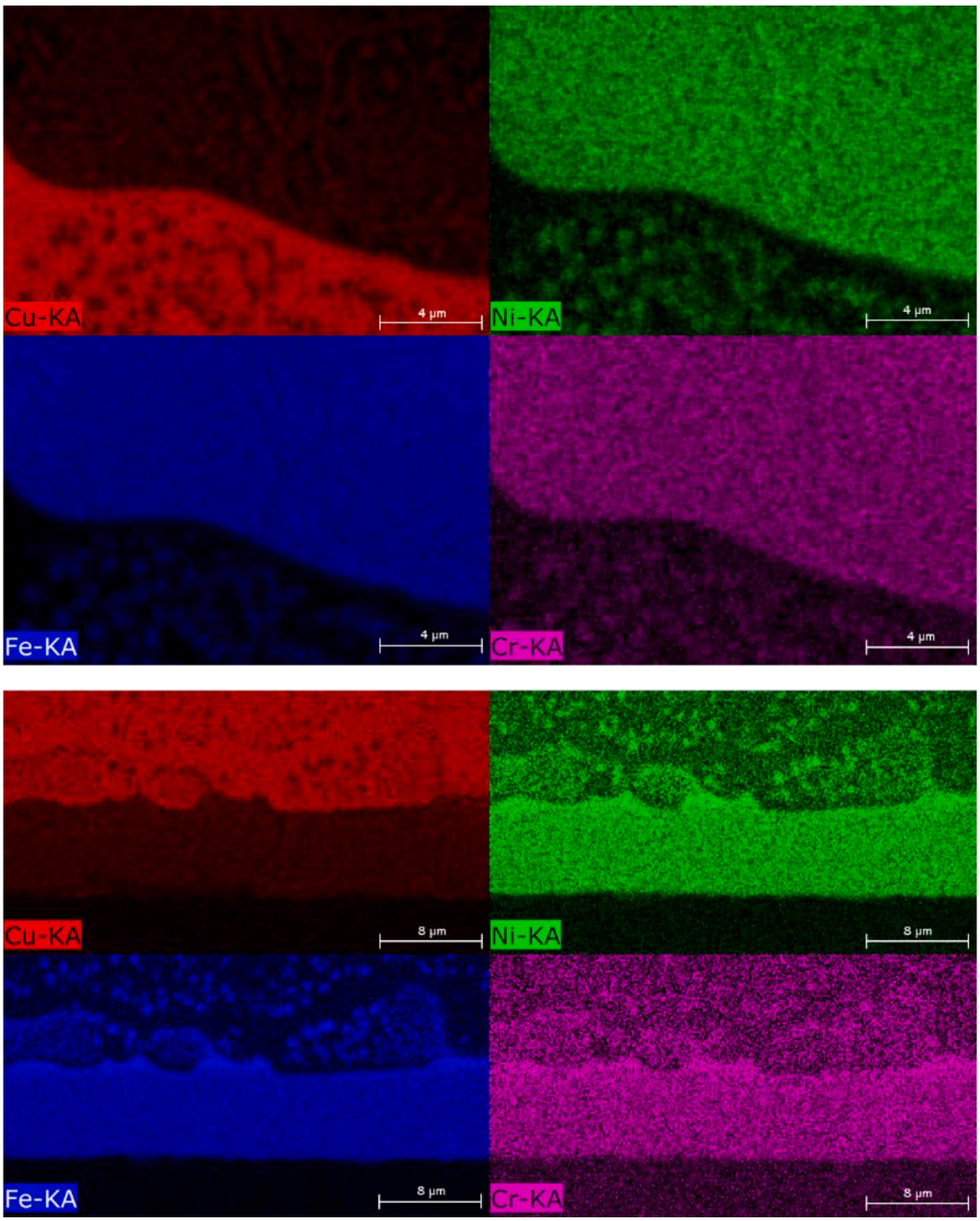

Fig. 8. EDS Chemical composition of a) EUROFER 97 and b) tungsten interfaces after brazing.

interface, which theoretically melts at around 1200 °C. The phase diagram shows that, as expected, compositions at 3 and 4 have formed from the liquid phase since melting occurs, while composition at 2 may have formed by solid-state diffusion mechanism.

4.2. Mechanism formation and microstructural evolution of W-W joints

A lower level of diffusion phenomenon and metallurgical interaction between braze and base materials was observed in these joints. The lowest brazed temperature joint is characterized by a defined interface, where braze and base material are easily identified and separated.

In the 1190 °C brazed joint, some incorporation of W into the braze with spherical geometry (highlighted with a red box in Fig. 11b) was detected. Its morphology and location, close to the W-Cu10Ni interface, indicates that constitutional liquefaction could have occurred at the W base material grain boundaries in contact with the braze, where Ni diffuses through the tungsten grain boundaries. This liquefaction phenomenon could have led to a partial dilution of the grain boundary, and once the dilution process has surrounded the whole grain, it leads to its incorporation into the brazed joint. The Ni–W phase diagram shows a decrease in the melting point from 3410 °C of pure tungsten 3410 °C (100 at.% W) to 1498 °C at the eutectic point (45 at.% W). Therefore, it would be necessary to consider the participation of other elements that would further reduce the melting temperature to the values reached during the imposed thermal cycle (1190 °C).

4.3. Mechanical properties evaluation

According to the results shown in Fig. 13, tungsten's mechanical properties (more specifically, its hardness value) have not been modified

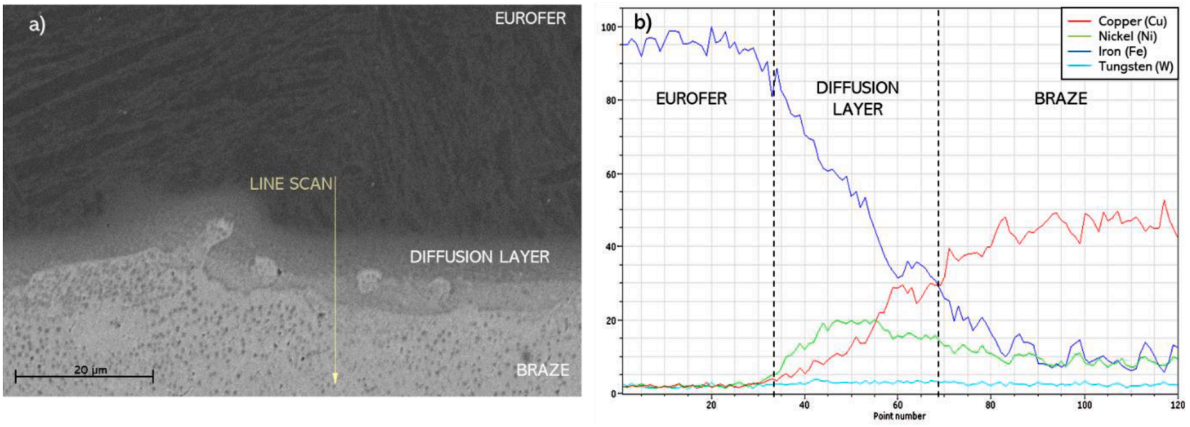

Fig. 9. a) SEM micrograph of E-Cu10Ni interface showing the line path and b) the chemical element distribution (at.%.) along the path.

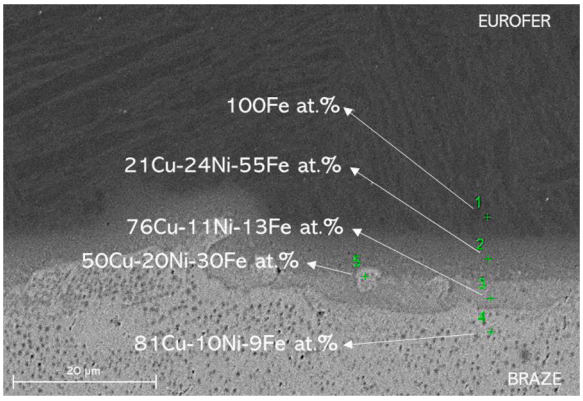

Fig. 10. Punctual analysis was carried out through the E-Cu10Ni interface of the brazed joint at 1190 °C.

after the different brazing processes. This is due to its inherent higher melting and recrystallization temperatures, which confer an inherent character at these temperatures and, therefore, have minimal variation on its microstructure.

On the other hand, EUROFER 97 undergoes a hardening process compared to the as-receive value, which could be attributed to the resultant microstructure after the brazing process, which in this case, is untempered martensite. Therefore, it will be necessary to perform a tempering process to restore the microstructure and hardness of the material.

The difference in EUROFER 97 hardness values subjected to different thermal cycles is related to the steel grain size generated. The higher the brazing temperature is, the coarser the austenitic grain is produced and, therefore, lower hardness values are obtained. The observation of this phenomenon when measuring hardness value and grain size after applying annealing treatments to EUROFER from 850 to 1120 °C. Above 1000 °C, the hardness values decreased, associated with grain size growth and recrystallization processes before quenching [25]. According to the study grain sizes of 14,3 µm to 52,5 µm were obtained for annealing temperatures of 1000 and 1120 °C, respectively.

In the case of the Cu10Ni filler lower hardness values compared the as-received properties were obtained. It may be associated with the restoration effect of the melting process and the low cooling ramp used, which may not achieve the original manufacturing processing microstructure and a larger grain size is obtained.

Regarding the shear tests shown in Fig. 14, the slightly lower values of W-E joints compared to W-W could be associated with the less metallurgical interaction of the latter, which results in the formation of a continuous solid solution braze with less presence of brittle phases. The reason could be associated with the inert metallurgical character of W at those temperatures that produces, in all cases, a well-defined interface. According to the residual stresses simulation results of Section 4.4, which will be discussed later, the residual stresses generated during the brazing process are accumulated at this point, and the brittle character of tungsten leads to the nucleation and initiation of the crack propagation.

In all conditions, cracks were initiated and propagated through the W-Cu10Ni interface. The reason could be associated with the lesser diffusion of elements between tungsten and the brazing filler. EUROFER 97 has greater diffusion, as previously mentioned and discussed, so stronger, nickel-richinterfaces than the W-Cu10Ni are formed. In W-E joints, as temperature increases the shear strength increases as well, while in W-W joints, temperature has an inverse effectwhich agrees with the explanation of the liquefaction effect in the W grain boundaries. The

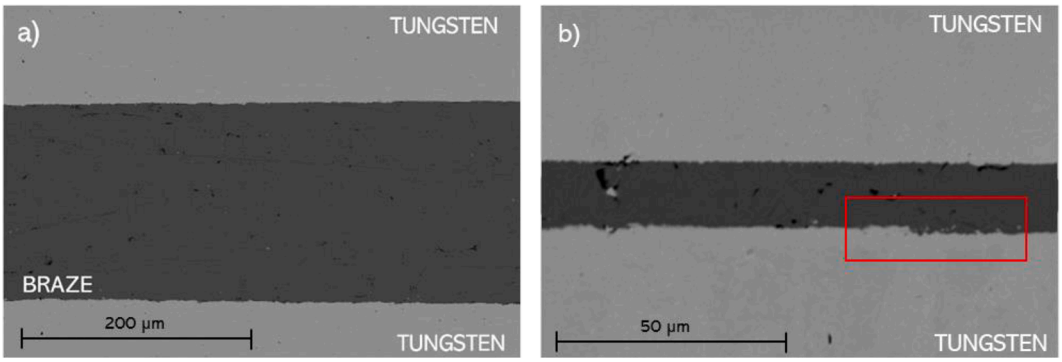

Fig. 11. SEM micrographs of W-W joints brazed with Cu10Ni commercial filler at a) 1165 °C and b) 1190 °C.

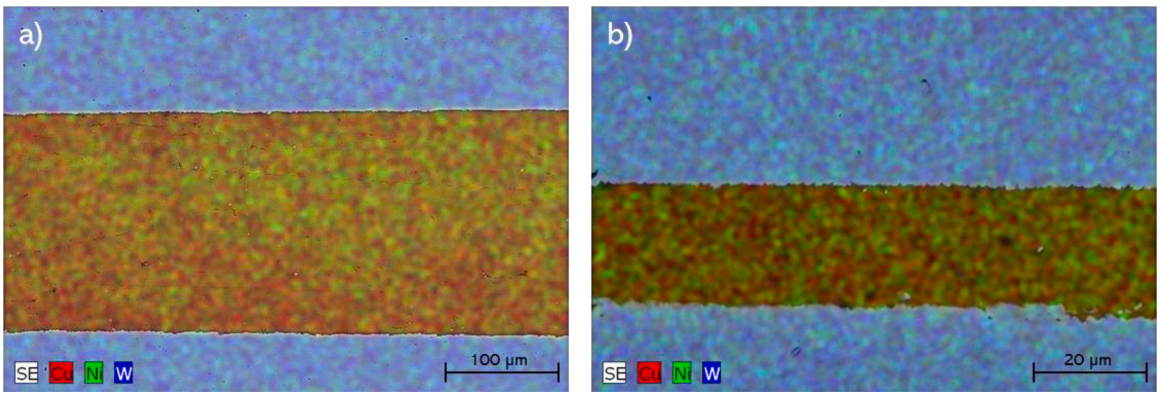

Fig. 12. EDX mapping showing general element distribution on W-W joint brazed at a) 1165 °C and b) 1190 °C.

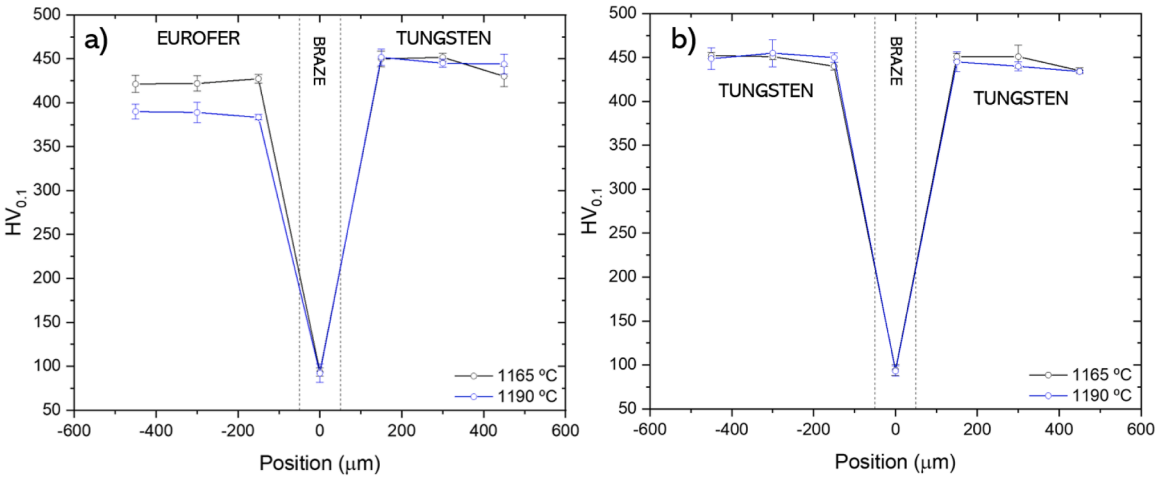

Fig. 13. Vickers hardness profile in a) W-E joints brazed at 1190 °C and b) W-W joints brazed at 1165 °C and 1190 °C.

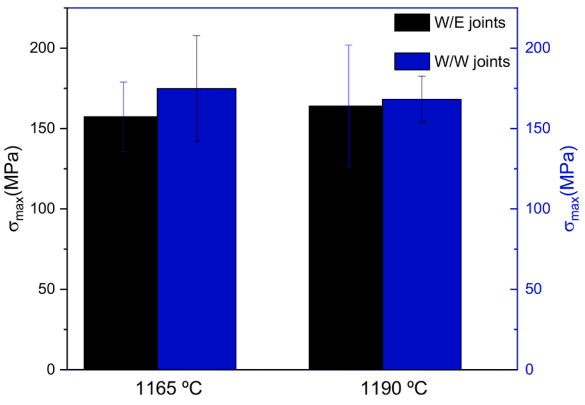

Fig. 14. Brazed joints shear values for W-E and W-W brazed joints.

microstructural analysis in Sections 3.2 and 3.3 revealed that higher brazing temperatures led to more braze penetration in the tungsten grain boundaries by constitutional liquefaction mechanism, which weakens the interface and acts as stress concentration points, where cracks can be quickly initiated and propagated at lower loads.

4.4. FEM post-brazing residual stresses analysis

4.4.1. W-E joints

Considering the importance of the residual stress in this heterogeneous joint, as previously mentioned in the fracture analysis, that causes the initiation and propagation of cracks during mechanical tests, this section aims to simulate and discuss the residual stress generated on both base material and the braze after the application of the brazing process. In this section FE analysis will be carried out with the pre-processing as commented on in Section 2.5. Fig. 17 shows the normal stress values in the X and Y axes after the cooling step of the brazed cycle. According to the results, Cu10Ni is subjected to a high tensile stress value on the X-axis. Considering that Cu10Ni has a higher CTE value than all involved materials, during the cooling phase, the filler tends to experience with higher shrinkage than EUROFER 97 and tungsten; therefore, the filler is subjected to a positive value of stress. The maximum value of this positive stress experienced by the filler material would be at the W-Cu10Ni interface due to the higher difference in its CTE. The analysis of the stress value in the Y-axis indicates that the maximum value is found at the edges of the braze. Therefore, those zones seem critical from the residual stress concentration point of view, acting as concentration points, which could lead to the nucleation and initiation of cracks.

Fig. 18 shows the distribution of the stress values for the X and Y axis of the braze, both interfaces, and the nearest zone of the base material. According to the previous result, those zones are considered the most relevant to be analyzed. At the W-Cu10Ni interface, the stress reaches 337 MPa in tensile mode, while at the E-Cu10Ni interface, the stress reaches a value of 326 MPa in tensile mode, which could be explained due to the greater difference in CTEs between the tungsten base material and the filler alloy.

Considering the materials studied as elastic and linear non-auxetic materials, Hooke's law explains the relationship between the stresses

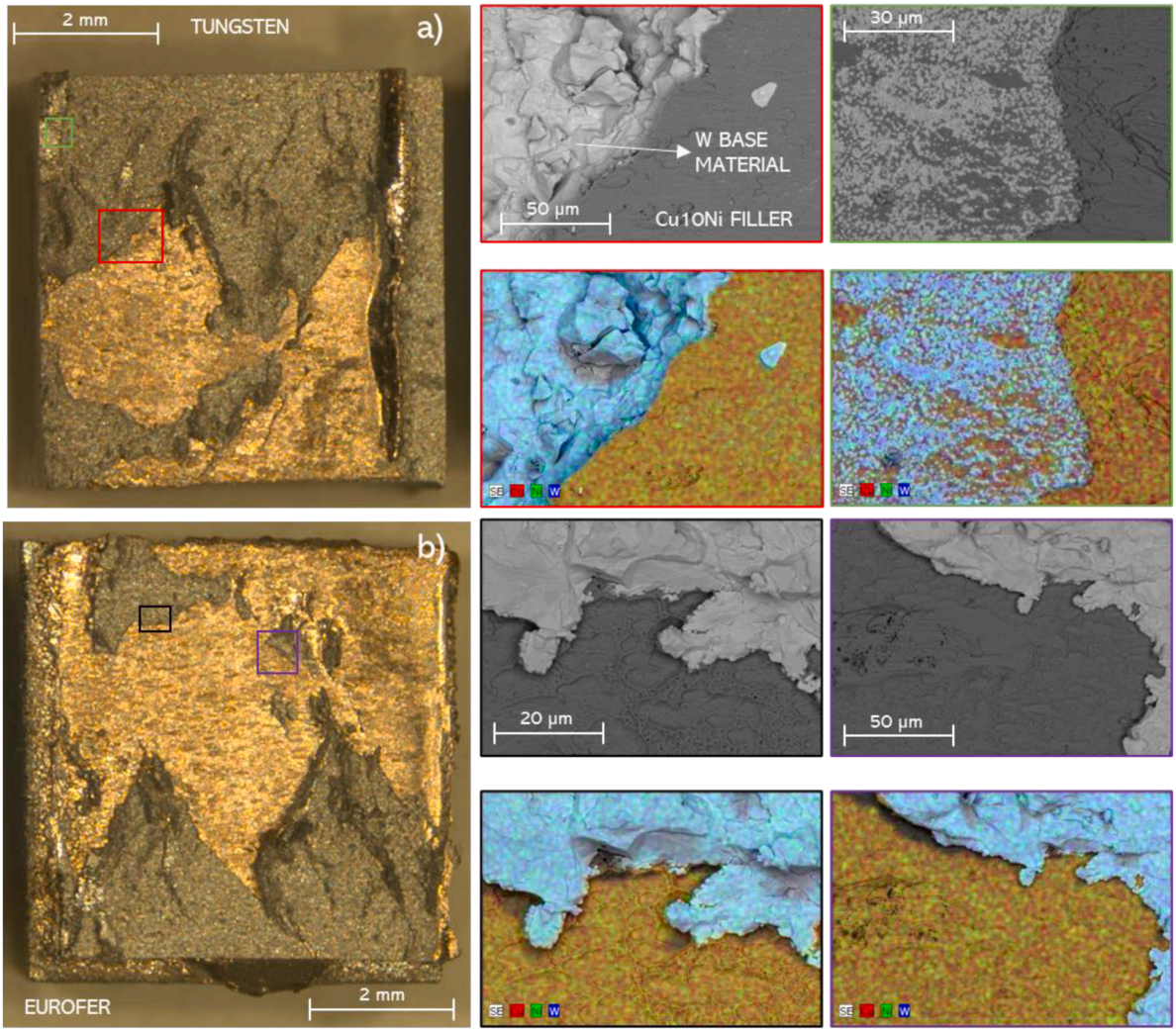

Fig. 15. Fracture surface analysis in both a) tungsten and b) EUROFER 97 base materials from 1165 °C conditions.

in the X and Y directions, where:

$$\varepsilon_Y = \frac{1}{E}\cdot(\sigma_Y - \upsilon\sigma_X)$$

Where $\sigma_Z = 0$ and no tangential contributions are present due to the 2D model design, this leads the stress value in the axis to depend on stress in the X-axis as follows:

$$\sigma_Y = E\cdot\varepsilon_Y - \upsilon\cdot\sigma_X$$

E and υ are isotropic material elastic constants, and ε is almost zero due to the bonded interfaces with base materials, which prevent Cu10Ni from shrinkage.

4.4.2. *W-W joints*

The same analysis was conducted with joints between tungsten (W-W) using the same cooling ramp and filler. Fig. 19 shows the same normal stresses analyzed previously in the W-E joint, with all range values and contours. Again, lower stress values are calculated at the joint edges The global distribution of the stresses follows a similar pattern to that studied in the previous joints, where the edges of the joint play an important role. Here, the top and bottom base materials are the same, so symmetry in the stress distribution is observed at both interfaces due to the same CTE of both base materials.

Fig. 20 shows the same stress values distribution for the X and Y axes along the vertical path focusing on the critical zones close to the interface area. Cu10Ni has a value of 319,3 MPa in both interfaces, as the base materials are the same pure tungsten.

To finish the analysis, maximum, middle, and minimum stresses in principal directions are shown below in Fig. 21, which shows the distribution of these principal stresses along the same vertical path at the end of the cooling process for both the W-E and W-W joints. Interfaces suffer from high stresses due to the tendency of the filler to contract more than the base materials and the impediment that these aspects generate due to the bonding.

The Von Mises stresses for each material at the Cu10Ni interface are 341 MPa for W-E joints and 342,15 MPa for W-W joints. For the base materials, regardless of the type of joint, the Von Mises stresses at the different points of the bulk material (excluding the interfaces mentioned above) do not exceed 50 MPa. It is expected that, according to the variation of the yield strength with temperature, which is 645, 107, and 100 MPa at 750 °C for tungsten, EUROFER 97 and Cu10Ni, respectively, most of the residual stress is accumulated in Cu10Ni during the cooling ramp.

During the FE analysis, the stress distribution and the Von Mises stress values confirmed that interfaces are critical zones, and the presence of brittle components or abrupt interfaces could be detrimental to the mechanical integrity of the joint. Furthermore, the highest residual stress is concentrated in the W-Cu10Ni interface, which explains the observed fracture mechanism of the brazed joints during the shear tests.

Sharma et al. [32] carried out a similar FE analysis with a 2D planar

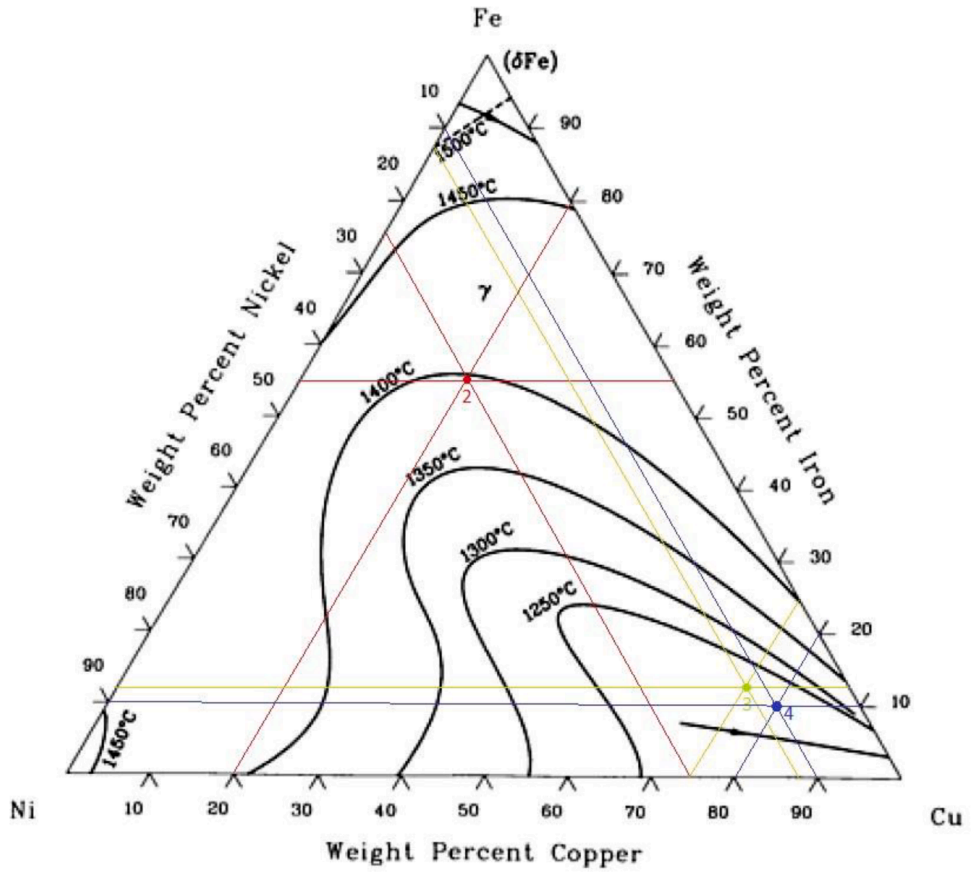

Fig. 16. Fe-Cu-Ni ternary phase diagram liquidus projection with points 2, 3, and 4 of the punctual analysis are marked [31].

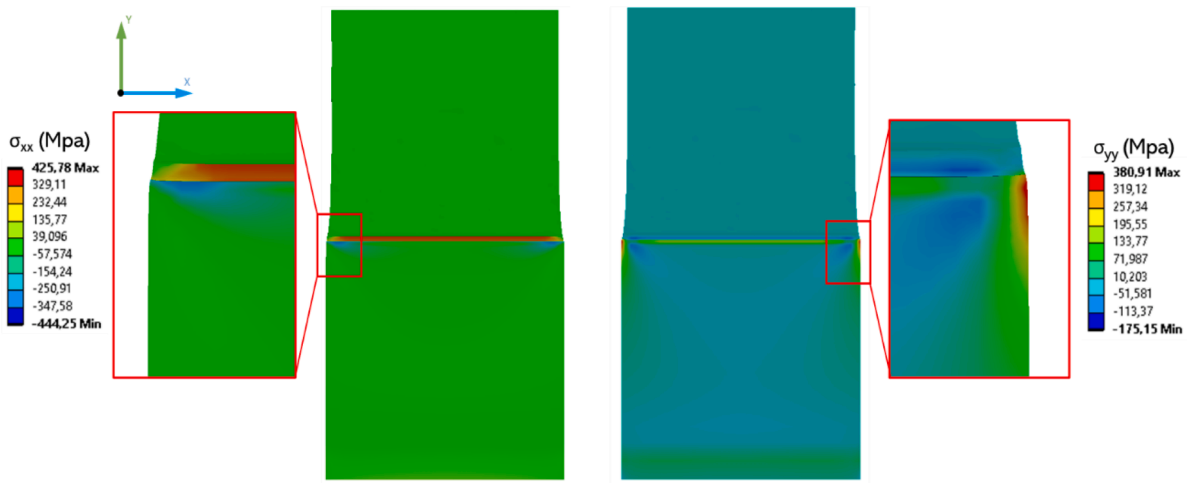

Fig. 17. After brazing for all materials involved (W-E joint), stress values and contours in the X and Y axes.

axisymmetric brazed joint geometry between Al_2O_3 and Kovar (Ni- and Co-based alloy) with TiCuSi alloy as filler. A cooling ramp from 780 °C to RT was imposed as the thermal condition, with frictionless support as the boundary condition. They found that the maximum tensile stress in the Y axis is 449,7 MPa, located in the brazing material of the joint, similar to that found in the present study (as shown Fig. 17).

Bobzin et al. [33] also studied the residual stresses on joints between steel and cemented carbide using copper foil as filler material. They applied a cooling ramp from 690 °C with no thermal gradient inside the materials ($\Delta T = 0$), with no phase transformations and constant chemical composition of substrates. Their model showed that the residual stresses in the steel (top base material) are very low, compared with the internal stresses in the cemented carbide (bottom base material) and the filler metal, which represent a significant preloading of the joint ($\simeq$ 600 MPa). The brazing foils with Cu-interlayer results generally show a reduction of the residual stresses in the cemented carbide compared to the conventional brazing foils due to their ductile behavior.

5. Conclusions

The commercial alloy Cu10Ni has been evaluated as a filler for joining tungsten (W) to itself (W-W) and to other materials (W-E) using

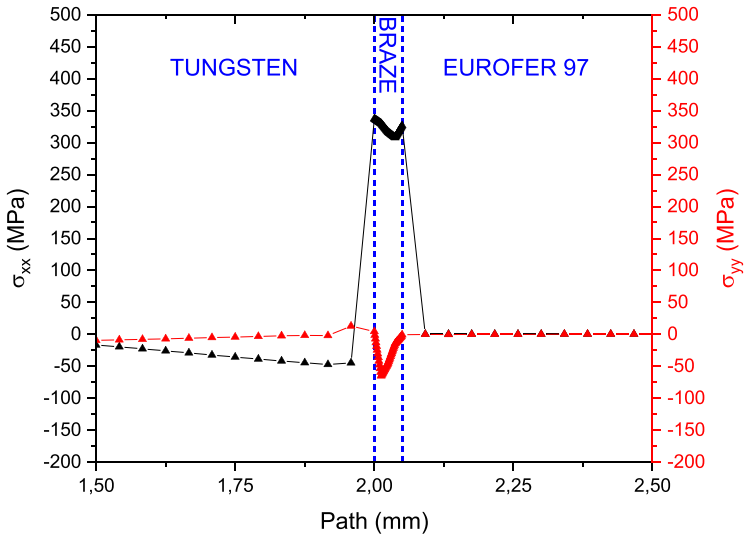

Fig. 18. Normal stress values for all three materials (W-E joint) during the cooling ramp through a vertical path along the three materials.

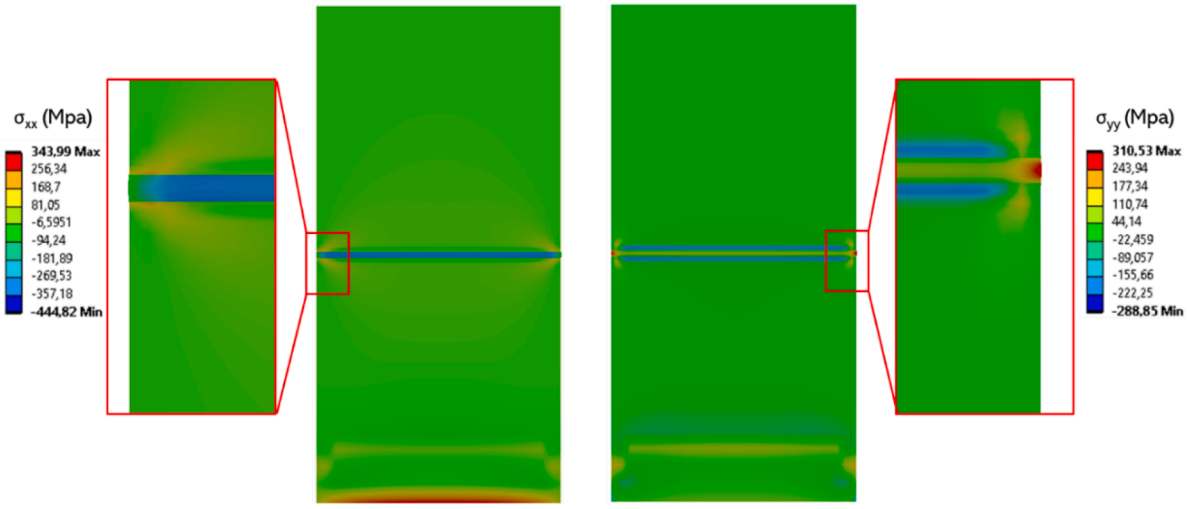

Fig. 19. After brazing for all materials involved (W-W joint), stress values and contours in the X and Y axes.

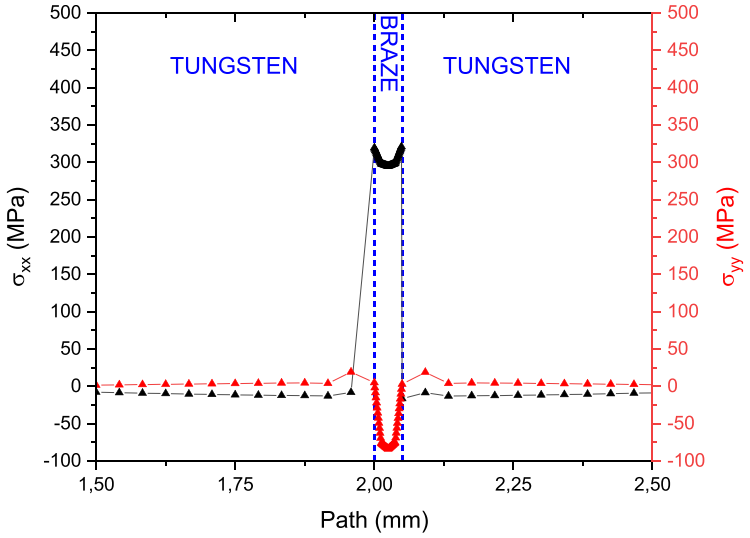

Fig. 20. Normal stress values for all three materials (W-W joint) during the cooling ramp through a vertical path along the three materials.

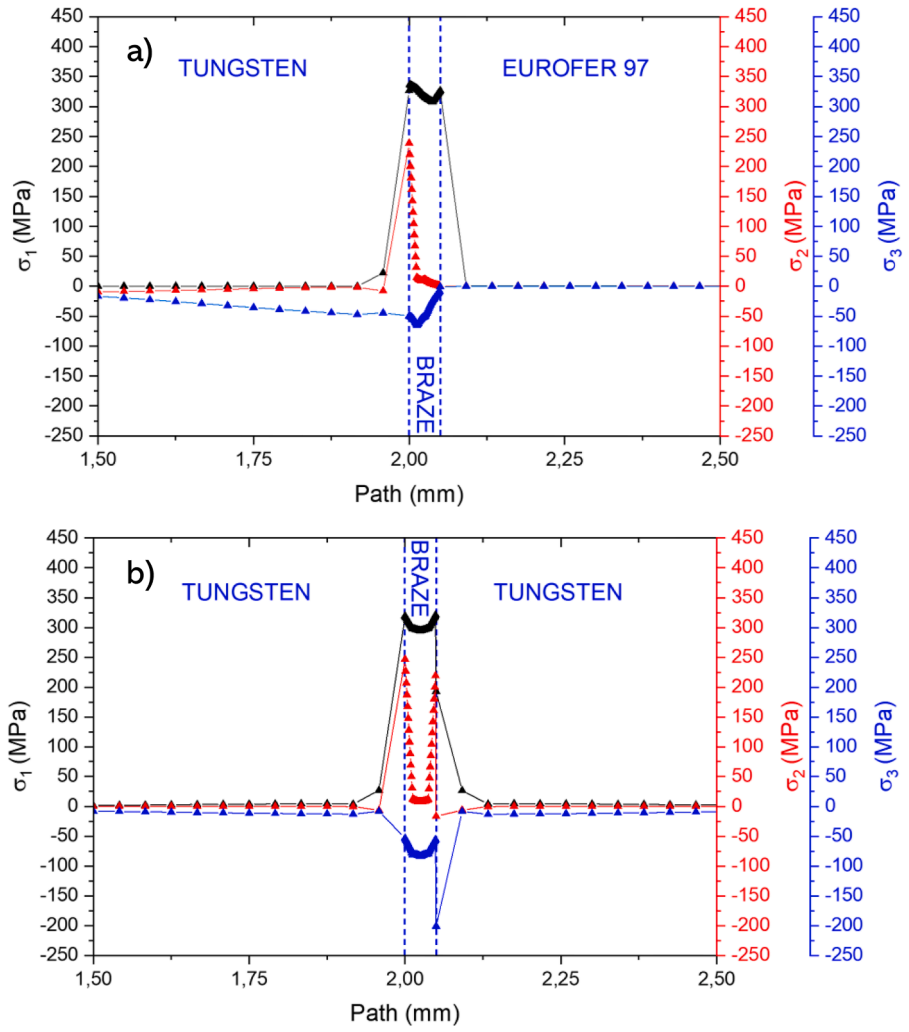

Fig. 21. Principal stress (black = σ1, red = σ2, and blue = σ3) values for all three materials in a) W-E and b) W-W joints during the cooling ramp through a vertical path along the three materials.

brazing. Two brazing cycles were tested, one at 25 °C above the liquidus temperature of the filler alloy and one at 50 °C above the liquidus temperature.

Microstructural analysis of the joints showed that total metallurgic solderability was achieved with little to no defects and complete interaction between the materials. A diffusion region of approximately 15 μm rich in nickel with rod-like copper-rich isolated eutectics was found in W-E joints at the E-Cu10Ni interface. The active character of Ni and the Fe dissolution explain the formation of those secondary phases. An increase in the brazing temperature enhances those phenomena, and stronger interfaces are formed, according to the shear tests carried out after the microstructural study.

W-W joints showed less severe diffusion and interaction between elements, but some spherical W particles were incorporated into the filler. A phenomenon of constitutional liquefaction occurred, where nickel diffuses through the grain boundary of the tungsten, originating a partial dilution of the grain boundary and the consequent introduction of the grain into the brazed joint. The Ni-W phase diagram and scientific literature supported this. As the shear test demonstrated, increasing this phenomenon as the brazing temperature increases weakens the interface integrity.

Microhardness profiles obtained across the brazing joints showed that EUROFER 97 base material experienced a hardening effect (423 ± 3 $HV_{0.1}$ for 1165 °C and 382 ± 2 $HV_{0.1}$ for 1190 °C) associated with the thermal brazing cycle. The austenitizing temperature is always reached and quenched from that state, which leads to the formation of untampered martensite microstructure, and the higher the brazing temperature, the softer the material is because of the austenitic grain growth. The Cu10Ni braze decreased its hardness with the thermal cycle (148 ± 10 $HV_{0.1}$ before lamination vs 93,6 ± 5 $HV_{0.1}$ for 1165 °C and 92,1 ± 11 $HV_{0.1}$ for 1190 °C).

Shear tests carried out in W-E joints showed higher values (174 MPa for 1165 °C and 168 MPa for 1190 °C) than the W-W joints (157 MPa for 1165 °C and 164 MPa for 1190 °C). The lower strength obtained for the W-W joints could be associated with the formation of abrupt interfaces, favoring the stress concentration, as demonstrated by the simulation of the residual stress in the brazed joints after the brazing process. The fracture mechanisms study corroborates this conclusion during the shear tests, which showed a fracture initiated and propagated through the W-Cu10Ni interface.

Regarding this study, the maximum principal stress values at the interfaces and across the filler did not vary excessively between W-E or W-W joints. The filler was subjected to positive stress values on the X-axis and compression values on the Y-axis, resulting in a Von Mises equivalent stress consistently higher than its yield stress. Stress values of around 60 MPa for the bottom base material and around 320 MPa for the filler alloy in the Y-axis are observed at the end of the thermal ramp. The information provided by the simulation shows the importance of mitigating the residual stress by selecting an adequate the filler alloy in terms of CTE or alloys capable of relieving the residual stress by plastic

deformation mechanisms.

CRediT authorship contribution statement

V. Díaz-Mena: Conceptualization, Data curation, Formal analysis, Investigation, Methodology, Writing – original draft. **J. de Prado:** Conceptualization, Formal analysis, Investigation, Supervision, Writing – review & editing, Funding acquisition, Methodology. **M. Roldán:** Resources, Writing – review & editing. **I. Izaguirre:** Methodology, Supervision, Writing – review & editing. **M. Sánchez:** Conceptualization, Funding acquisition, Resources, Supervision, Writing – review & editing, Project administration, Validation. **M. Rieth:** Conceptualization, Funding acquisition, Resources, Project administration. **A. Ureña:** Conceptualization, Funding acquisition, Project administration, Supervision, Validation, Writing – review & editing.

Declaration of Competing Interest

The authors declare that they have no known competing financial interests or personal relationships that could have appeared to influence the work reported in this paper.

Data availability

Data will be made available on request.

Acknowledgments

This work has been carried out within the framework of the EUROFusion Consortium, funded by the European Union via the Euratom Research and Training Programme (Grant Agreement No. 101052200 — EUROfusion). Views and opinions expressed are however those of the author(s) only and do not necessarily reflect those of the European Union or the European Commission. Neither the European Union nor the European Commission can be held responsible for them. The authors acknowledge the use of instrumentation and the technical advice provided by the Facility ICTS, node "Laboratorio de Microscopías y Análisis de Superficie" at the CIEMAT.

References

[1] G. Federici, J. Holden, C. Baylard, A. Beaumont, The EU DEMO staged design approach in the Pre-concept design phase, Fusion Eng. Des. 173 (2021), https://doi.org/10.1016/j.fusengdes.2021.112959.
[2] M. Gorley, G. Aiello, J. Henry, T. Nozawa, G. Pintsuk, M. Rieth, H. Tanigawa, DEMO structural materials qualification and development, Fusion Eng. Des. 170 (2021), https://doi.org/10.1016/j.fusengdes.2021.112513.
[3] S.J. Zinkle, J.T. Busby, Structural materials for fission & fusion energy, Mater. Today 12 (2009) 12–19, https://doi.org/10.1016/S1369-7021(09)70294-9.
[4] M. Gorley, E. Diegele, S. Dudarev, G. Pintsuk, Materials engineering and design for fusion—towards DEMO design criteria, Fusion Eng. Des. 136 (2018) 298–303, https://doi.org/10.1016/J.FUSENGDES.2018.02.012.
[5] D. Stork, P. Agostini, J.L. Boutard, D. Buckthorpe, E. Diegele, S.L. Dudarev, C. English, G. Federici, M.R. Gilbert, S. Gonzalez, A. Ibarra, C. Linsmeier, A. L. Puma, G. Marbach, L.W. Packer, B. Raj, M. Rieth, M.Q. Tran, D.J. Ward, S. J. Zinkle, Materials R&D for a timely DEMO: key findings and recommendations of the EU roadmap materials assessment group, Fusion Eng. Des. 89 (2014) 1586–1594, https://doi.org/10.1016/J.FUSENGDES.2013.11.007.
[6] J.W. Coenen, Y. Mao, S. Sistla, A.V. Müller, G. Pintsuk, M. Wirtz, J. Riesch, T. Hoeschen, A. Terra, J.H. You, H. Greuner, A. Kreter, C. Broeckmann, R. Neu, C. Linsmeier, Materials development for new high heat-flux component mock-ups for DEMO, Fusion Eng. Des. 146 (2019) 1431–1436, https://doi.org/10.1016/J.FUSENGDES.2019.02.098.
[7] R. Lindau, M. Schirra, First results on the characterisation of the reduced-activation-ferritic-martensitic steel EUROFER, Fusion Eng. Des. 58–59 (2001) 781–785, https://doi.org/10.1016/S0920-3796(01)00562-2.
[8] E. Wakai, T. Sawai, A. Naito, S. Jitsukawa, Microstructural development and swelling behaviour of F82H steel irradiated by dual ion beams, Microscopy 51 (2002) S239–S243, https://doi.org/10.1093/jmicro/51.Supplement.S239.
[9] Z. Chen, X. Hu, M. Ye, B.D. Wirth, Deuterium transport and retention properties of representative fusion blanket structural materials, J. Nucl. Mater. 549 (2021), 152904, https://doi.org/10.1016/J.JNUCMAT.2021.152904.
[10] L.C. Alves, E. Alves, A. Paúl, M.R. da Silva, J.A. Odriozola, Ion beam characterisation of ODS steel samples after long term annealing conditions, Nucl. Instrum. Methods Phys. Res. B 249 (2006) 493–496, https://doi.org/10.1016/J.NIMB.2006.03.038.
[11] C. Linsmeier, M. Rieth, J. Aktaa, T. Chikada, A. Hoffmann, J. Hoffmann, A. Houben, H. Kurishita, X. Jin, M. Li, A. Litnovsky, S. Matsuo, A. Von Müller, V. Nikolic, T. Palacios, R. Pippan, D. Qu, J. Reiser, J. Riesch, T. Shikama, R. Stieglitz, T. Weber, S. Wurster, J.H. You, Z. Zhou, Development of advanced high heat flux and plasma-facing materials, Nucl. Fusion. 57 (2017), https://doi.org/10.1088/1741-4326/aa6f71.
[12] M. Gorley, E. Diegele, E. Gaganidze, F. Gillemot, G. Pintsuk, F. Schoofs, I. Szenthe, The EUROfusion materials property handbook for DEMO in-vessel components—status and the challenge to improve confidence level for engineering data, Fusion Eng. Des. 158 (2020), https://doi.org/10.1016/j.fusengdes.2020.111668.
[13] B.A. Kalin, V.T. Fedotov, O.N. Sevrjukov, A.N. Kalashnikov, A.N. Suchkov, A. Moeslang, M. Rohde, Development of brazing foils to join monocrystalline tungsten alloys with ODS-EUROFER steel, J. Nucl. Mater. 367–370 (2007) 1218–1222, https://doi.org/10.1016/J.JNUCMAT.2007.03.222.
[14] J. de Prado, M. Sánchez, M. Wirtz, G. Pintsuk, J. Du, J. Linke, A. Ureña, Impact of thermal fatigue on W–W brazed joints for divertor components, J. Mater. Process. Technol. 252 (2018) 211–216, https://doi.org/10.1016/J.JMATPROTEC.2017.09.024.
[15] C.C. Zhu, Y.T. Song, X.B. Peng, Y.P. Wei, X. Mao, W.X. Li, X.Y. Qian, The dynamical mechanical properties of tungsten under compression at working temperature range of divertors, J. Nucl. Mater. 469 (2016) 120–124, https://doi.org/10.1016/J.JNUCMAT.2015.11.045.
[16] G. Arnoux, J. Coenen, B. Bazylev, Y. Corre, G.F. Matthews, I. Balboa, M. Clever, R. Dejarnac, S. Devaux, T. Eich, E. Gauthier, L. Frassinetti, J. Horacek, S. Jachmich, D. Kinna, S. Marsen, P. Mertens, R.A. Pitts, M. Rack, G. Sergienko, B. Sieglin, M. Stamp, V. Thompson, Thermal analysis of an exposed tungsten edge in the JET divertor, J. Nucl. Mater. 463 (2015) 415–419, https://doi.org/10.1016/J.JNUCMAT.2014.11.005.
[17] Q. Cai, W. Liu, Y. Ma, Z. Wang, Diffusion brazing of tungsten and steel using Ti-Ni liquid phase forming interlayer, Fusion Eng. Des. 91 (2015) 67–72, https://doi.org/10.1016/j.fusengdes.2014.12.029.
[18] A. Levy, Thermal residual stresses in Ceramic-to-Metal brazed joints, J. Am. Ceram. Soc. 74 (1991) 2141–2147, https://doi.org/10.1111/j.1151-2916.1991.tb08273.x.
[19] I. Izaguirre, M. Roldán, J. de Prado, V. Bonache, M. Sánchez, A. Ureña, S/TEM examination and nanomechanical response of W-Eurofer joints brazed with Cu interlayers, Nucl. Mater. Energy 31 (2022), https://doi.org/10.1016/j.nme.2022.101155.
[20] D. Bachurina, A. Suchkov, A. Filimonov, I. Fedotov, M. Savelyev, O. Sevryukov, B. Kalin, High-temperature brazing of tungsten with steel by Cu-based ribbon brazing alloys for DEMO, Fusion Eng. Des. 146 (2019) 1343–1346, https://doi.org/10.1016/J.FUSENGDES.2019.02.072.
[21] D. Bachurina, A. Suchkov, J. Gurova, M. Savelyev, P. Dzhumaev, I. Kozlov, R. Svetogorov, M. Leont'eva-Smirnova, O. Sevryukov, Joining tungsten with steel for DEMO: simultaneous brazing by Cu-Ti amorphous foils and heat treatment, Fusion Eng. Des. 162 (2021), 112099, https://doi.org/10.1016/J.FUSENGDES.2020.112099.
[22] J. de Prado, M. Sánchez, I. Izaguirre, D. Swan, A. Ureña, Exploring Cu-Ge alloys as filler materials for high vacuum brazing application of W and CuCrZr, Mater Today Commun 33 (2022), https://doi.org/10.1016/j.mtcomm.2022.104286.
[23] Z. Zhong, H.C. Jung, T. Hinoki, A. Kohyama, Effect of joining temperature on the microstructure and strength of tungsten/ferritic steel joints diffusion bonded with a nickel interlayer, J. Mater. Process. Technol. 210 (2010) 1805–1810, https://doi.org/10.1016/j.jmatprotec.2010.06.012.
[24] M. Sánchez, M.A. Garrido, C.J. Múnez, J. Rams, A. Ureña, Analysis of the brazeability of W-W joints using a high temperature Ni-based alloy, Mater. Des. 54 (2014) 900–905, https://doi.org/10.1016/j.matdes.2013.08.106.
[25] M. Rieth, M. Schirra, A. Falkenstein, P. Graf, S. Heger, H. Kempe, R. Lindau, H. Zimmermann, EUROFER 97 Tensile, Charpy, Creep Struct.l Tests (2003).
[26] M. Li, S.J. Zinkle, Physical and mechanical properties of copper and copper alloys. Comprehensive Nuclear Materials, Elsevier Ltd, 2012, pp. 667–690, https://doi.org/10.1016/B978-0-08-056033-5.00122-1.
[27] B.K. Ehrlich, The development of structural materials for fusion reactors, n.d. https://royalsocietypublishing.org/.
[28] Erik. Lassner, W.-Dieter. Schubert, Tungsten : Properties, Chemistry, Technology of the Element, Alloys, and Chemical Compounds, Kluwer Academic/Plenum Publishers, 1999.
[29] A.A. Ivannikov, M.A. Penyaz, P.S. Dzhumaev, D.M. Bachurina, O.N. Sevriukov, Diffusion brazing of stainless steels influence of Ni-B filler alloy composition, Weld. World 65 (2021) 317–328, https://doi.org/10.1007/S40194-020-01013-Y/FIGURES/15.
[30] ASM International, ASM Handbook, Handbook Committee, 1990.
[31] Okamoto H., Schlesinger M.E., Mueller E.M., Alloy Phase Diagrams, n.d. https://doi.org/10.31399/asm.hb.v03.9781627081634.
[32] D.K. Sharma, M. Bandyopadhyay, J. Joshi, A.K. Chakraborty, Determination of Residual Stresses in Ceramic-Metal Brazed Joint using Finite Element Analysis (FEA) and Experimental Validation of the Results, SAMRIDDHI : J. Phys. Sci. Eng. Technol. 12 (2020) 1–7, https://doi.org/10.18090/samriddhi.v12i01.1.
[33] K. Bobzin, M. Öte, J. Hebing, Approaches and possibilities for reducing residual stresses in induction brazed cemented carbide/steel joints, Weld. World 64 (2020) 1579–1587, https://doi.org/10.1007/s40194-020-00928-w.